TECHNISCHE MECHANIK, 32, 1, (2012), 21 – 37
submitted: October 26, 2011

Computational Homogenization of Piezoelectric Materials using FE^2 to determine Configurational Forces

M. Khalaquzzaman, B.-X. Xu, S. Ricker, R. Müller

Due to the growing interest in determining the macroscopic material response of inhomogeneous materials, computational methods are becoming increasingly concerned with the application of homogenization techniques. In this work, two-scale classical (first-order) homogenization of electro-mechanically coupled problems using a FE^2-approach is discussed. We explicitly formulate the homogenized coefficients of the elastic, piezoelectric and dielectric tensors for small strain as well as the homogenized remanent strain and remanent polarization. The homogenization of the coupled problem is done using different representative volume elements (RVEs), which capture the microstructure of the inhomogeneous material, to represent the macro material response. Later this technique is used to determine the macroscopic and microscopic configurational forces on certain defects.

1 Introduction

The purpose of this work is to investigate the effects of the micro inhomogeneities of piezoelectric materials to the configurational force on macro level. Special attention is given on the configurational forces at certain defect situations. These defect situations include the configurational force at a sharp crack tip. To fulfill the task, one needs to deal with three broad fields of mechanics: electro-mechanically coupled piezoelectric material; computational homogenization of piezoelectric material; and configurational force theory. Piezoelectric material is widely used in sensing and actuation devices. This material is highly inhomogeneous on the micro level due to different domains of polarization, domain walls, grains, grain boundaries, micro cracks, etc. Inhomogeneities of the material on different scales are illustrated in Figure 1. For a detailed description of piezoelectric materials, readers are referred to the text books by Xu (1991) and Qin (2001).

It is rather difficult to accurately capture the macroscopic material responses only with pre-assumed overall constitutive relations. To have the overall macro material response of microscopically inhomogeneous material, we need to use some kind of homogenization techniques. There are several homogenization or multiscale techniques, e.g., asymptotic homogenization, semi-analytical homogenization, computational homogenization (FE^2 based or Fourier transformation based homogenization), see Kanouté et al. (2009). The first two homogenization methods are only applicable to simple microstructure, while the computational homogenization technique is suitable for more complex micro domain. To have a comprehensive overview on overall properties of heterogeneous materials, see for instance the paper by Hill (1972) and the textbook by Nemat-Nasser and Hori (1993). A comprehensive survey on homogenization techniques can also be found in Kanouté et al. (2009). Homogenization of piezoelectric materials based on FE^2-approach can be found in Schröder (2009), Schröder and Keip (2010, 2011). To capture the effect of the micro inhomogeneities on the configurational force on macro level, one also needs to homogenize the Eshelby stress tensor. Several approaches for large deformation problem are proposed in Ricker et al. (2010). As large deformation are not present in piezoelectric materials, we used the averaging technique for small deformations to get the homogenized Eshelby stress tensor.

Eshelby (1951) introduced the concept of the energy-momentum tensor in continuum mechanics of solids, although at that time Eshelby did not use the term energy-momentum tensor, but preferred the expression Maxwell-tensor of elasticity. The term energy-momentum tensor was introduced later, see Eshelby (1970). Configurational forces, which can be interpreted as the energy changes in the system, are a convenient tool to investigate inhomogeneities or fracture of solids. Further, this physical quantity was also used in refinement of finite element meshing in Müller and Maugin (2002), Müller et al. (2002) and Braun (1997). To get a more detailed idea on configurational forces, readers are referred to Maugin (1993), Maugin (2010), Kienzler and Herrmann (2000), Gurtin (1995) and Gurtin (2000). The nodal configurational forces represent the defect driving forces, e.g., the configurational force at a

crack tip corresponds to the J-integral proposed by Rice (1968). Thus, the magnitude of the configurational crack tip force yields a criterion whether a crack propagates.

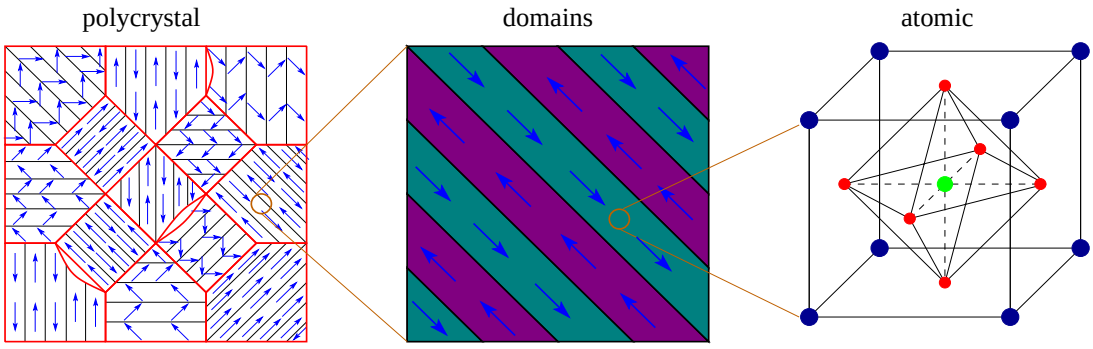

Figure 1: *Illustration of piezoelectric materials on different scales*

2 Theory of Piezoelectric Material

2.1 Field Equations

We consider a piezoelectric body $\mathcal{B}$ which contains domain walls and domains. The normal $\mathbf{n}_\mathcal{S}$ to a domain wall $\mathcal{S}$ points from the sub-body $\mathcal{B}^-$ into $\mathcal{B}^+$, for details see Figure 2. Neglecting the inertia term the Cauchy stress tensor $\boldsymbol{\sigma}$ fulfills the mechanical equilibrium condition. The mechanical equilibrium has the form

$$\begin{aligned} \operatorname{div}\boldsymbol{\sigma} + \mathbf{f} &= \mathbf{0} \quad \text{in} \quad \mathcal{B}, \\ [\![\boldsymbol{\sigma}]\!]\mathbf{n}_\mathcal{S} &= \mathbf{0} \quad \text{on} \quad \mathcal{S}, \end{aligned} \tag{1}$$

in the bulk considering the volume force $\mathbf{f}$ and on the domain wall, respectively.

The operator $[\![(\cdot)]\!]$ in (1) is the jump operator. The mechanical problem must be supplemented with suitable boundary conditions. Prescribing either the displacements $\mathbf{u}^*$ on the boundary $\partial\mathcal{B}_u$ or the traction $\mathbf{t}^*$ on the boundary $\partial\mathcal{B}_t$, one has

$$\begin{aligned} \mathbf{u} &= \mathbf{u}^* \quad \text{on} \quad \partial\mathcal{B}_u, \\ \boldsymbol{\sigma}\mathbf{n} &= \mathbf{t}^* \quad \text{on} \quad \partial\mathcal{B}_t. \end{aligned} \tag{2}$$

The electric displacement vector $\mathbf{D}$ satisfies the electro-static relation (Gauss law). In the presence of the volume charges q, the field equations in the bulk and on the domain wall are

$$\begin{aligned} \operatorname{div}\mathbf{D} + q &= 0 \quad \text{in} \quad \mathcal{B}, \\ [\![\mathbf{D}]\!]\cdot\mathbf{n}_\mathcal{S} &= 0 \quad \text{on} \quad \mathcal{S}, \end{aligned} \tag{3}$$

respectively. One can prescribe either the electric potential φ^* or the surface charge Q^* on the boundary,

$$\begin{aligned} \varphi &= \varphi^* \quad \text{on} \quad \partial\mathcal{B}_\varphi, \\ \mathbf{D}\cdot\mathbf{n} &= -Q^* \quad \text{on} \quad \partial\mathcal{B}_Q. \end{aligned} \tag{4}$$

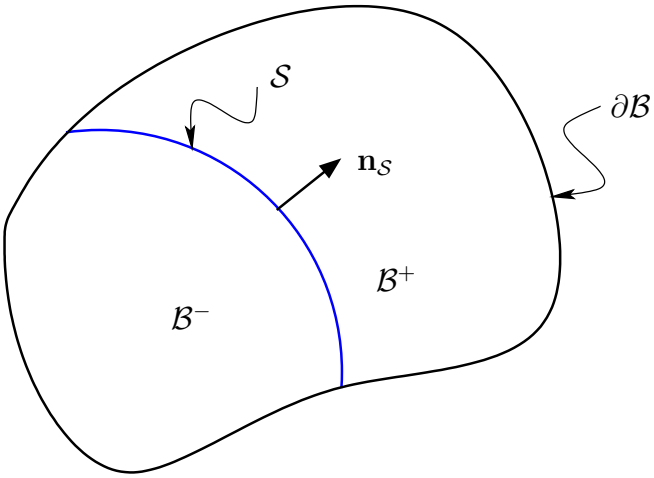

Figure 2: *Body containing a domain wall*

The kinematic relations in the bulk and on the domain wall are given by

$$\begin{aligned} \boldsymbol{\varepsilon} = \frac{1}{2}\left(\operatorname{grad}\mathbf{u} + (\operatorname{grad}\mathbf{u})^T\right) \quad &\text{in} \quad \mathcal{B}, \\ [\![\mathbf{u}]\!] = \mathbf{0} \quad &\text{on} \quad \mathcal{S}, \end{aligned} \tag{5}$$

where the linearized strain tensor $\boldsymbol{\varepsilon}$ is the symmetric part of the displacement gradient. The second relation indicates a continuous displacement across the domain wall. Thus, no separation, sliding, or interpenetration of the domains is allowed, see also Leo and Sekerka (1989). For the electric part, we need the following relations of the electric field $\mathbf{E}$ and electric potential φ,

$$\begin{aligned} \mathbf{E} = -\operatorname{grad}\varphi \quad &\text{in} \quad \mathcal{B}, \\ [\![\varphi]\!] = 0 \quad &\text{on} \quad \mathcal{S}. \end{aligned} \tag{6}$$

The electric field $\mathbf{E}$ is defined as the negative gradient of the electric potential φ. Across the domain wall, a continuous electric potential is assumed. All the field equations mentioned above are applicable for a boundary value problem (BVP) of the piezoelectric material on micro level. In case of a macro BVP all field equations except for the equations with jump operator should be taken into account, since we assume that the piezoelectric material is macroscopically homogeneous.

2.2 Piezoelectric Constitutive Law

To complete the field equations in the previous sections, constitutive relations, which bridge the Cauchy stress tensor $\boldsymbol{\sigma}$, the electric displacement vector $\mathbf{D}$ and the strain tensor $\boldsymbol{\varepsilon}$, the electric field $\mathbf{E}$, are needed. The material response of a ferroelectric ceramics under small electric or mechanical loading may be described by a linear piezoelectric constitutive law. One can write the electric enthalpy function as a thermodynamical potential,

$$\begin{aligned} H(\boldsymbol{\varepsilon}, \mathbf{E}) \quad = \quad & \frac{1}{2}(\boldsymbol{\varepsilon} - \boldsymbol{\varepsilon}^0){:}\left[\mathbb{C}(\boldsymbol{\varepsilon} - \boldsymbol{\varepsilon}^0)\right] - (\boldsymbol{\varepsilon} - \boldsymbol{\varepsilon}^0){:}(\mathbb{b}^T\mathbf{E}) \\ & -\frac{1}{2}\mathbf{E}\cdot(\mathbf{A}\,\mathbf{E}) - \mathbf{P}^0\cdot\mathbf{E} \end{aligned} \tag{7}$$

which comprises of an elastic, a coupling and an electric part. In the electric enthalpy function, $\mathbb{C}$ is the fourth order elastic tensor, $\mathbb{b}$ the third order piezoelectric tensor, $\mathbf{A}$ the second order dielectric tensor, $\boldsymbol{\varepsilon}^0$ the remanent strain, and $\mathbf{P}^0$ the remanent polarization. Taking the partial derivative with respect to $\boldsymbol{\varepsilon}$ and the negative of the partial derivative with respect to $\mathbf{E}$, one obtains expressions for the Cauchy stress tensor $\boldsymbol{\sigma}$ and the electric displacement $\mathbf{D}$,

$$\boldsymbol{\sigma} \quad = \quad \frac{\partial H}{\partial \boldsymbol{\varepsilon}} = \mathbb{C}(\boldsymbol{\varepsilon} - \boldsymbol{\varepsilon}^0) - \mathbb{b}^T\mathbf{E}, \tag{8}$$

$$\mathbf{D} \quad = \quad -\frac{\partial H}{\partial \mathbf{E}} = \mathbb{b}(\boldsymbol{\varepsilon} - \boldsymbol{\varepsilon}^0) + \mathbf{A}\,\mathbf{E} + \mathbf{P}^0, \tag{9}$$

2.3 Configurational Forces for Piezoelectric Materials

The theory of configurational forces, which are also known as material forces, gives an adequate tool for investigating the material behaviour with various kinds of material defects. The credit of making the introduction and calculating the configurational forces goes to the work of Eshelby in the early fifties of the 20th century. Configurational forces are interpreted as energy changes of the system. It is widely used in fracture mechanics and in phase transformations. For the derivation of the configuration force balance, we start from the gradient of H in (7). Making use of the mechanical balance law, kinematics, electrostatic, and the definition of electric field, the gradient of H leads to the balance of configurational force

$$\operatorname{div} \boldsymbol{\Sigma} + \mathbf{g} = \mathbf{0}, \tag{10}$$

where $\boldsymbol{\Sigma}$ is the electromechanical Eshelby stress tensor

$$\boldsymbol{\Sigma} = H\,\mathbf{1} - (\operatorname{grad} \mathbf{u})^T \boldsymbol{\sigma} - \operatorname{grad} \varphi \otimes \mathbf{D}$$

and $\mathbf{g}$ is the volume configurational force, expressed as

$$\mathbf{g} = \boldsymbol{\sigma} \colon \operatorname{grad} \boldsymbol{\varepsilon}^0 - (\operatorname{grad} \mathbf{u})^T \mathbf{f} + (\operatorname{grad} \varphi) q - \left. \frac{\partial H}{\partial \mathbf{x}} \right|_{\text{expl.}} \tag{11}$$

for electro-mechanically coupled problem. The notation expl. in (11) stands for the explicit derivative of the electric enthalpy H with respect to the position $\mathbf{x}$. Readers are referred to Maugin (2010), Kienzler and Herrmann (2000), Müller et al. (2006) and Schrade et al. (2007) for a detailed derivation of the electromechanical Eshelby stress tensor and the volume configurational force of piezoelectric material.

Finite element methods can be used to determine the nodal configurational forces in the discrete computational domain. The weak form of (10) is

$$\int_{\Omega} (\operatorname{div} \boldsymbol{\Sigma} + \mathbf{g}) \cdot \boldsymbol{\eta} \, \mathrm{d}\Omega = 0, \tag{12}$$

where $\boldsymbol{\eta}$ is a test function. After integration by parts,

$$\int_{\Omega} (-\boldsymbol{\Sigma} \colon \operatorname{grad} \boldsymbol{\eta} + \mathbf{g} \cdot \boldsymbol{\eta}) \, \mathrm{d}\Omega + \int_{\partial\Omega} \boldsymbol{\Sigma} \mathbf{n} \cdot \boldsymbol{\eta} \, \mathrm{d}\Gamma = 0, \tag{13}$$

where $\mathbf{n}$ is the normal vector on the boundary. Discretizing the volume integral in (13) by finite elements Ω_e and determining $\boldsymbol{\Sigma}$ at each Gauss point of the element, one can obtain the nodal configurational force at node I as

$$\mathbf{G}^I = \bigcup_{e\,=\,1}^{n_{\text{el}}^*} \int_{\Omega_e} \boldsymbol{\Sigma} \operatorname{grad} N^I \, \mathrm{d}\Omega, \tag{14}$$

where n_{el}^* is the total number of adjacent elements to node I and N^I is the corresponding shape function. It is possible to determine the nodal configurational forces without solving the balance equation of configurational force (10). Solving the standard balance equations and computing the required quantities, one can compute the Eshelby stress tensor. By using this Eshelby stress tensor in equation (14), one can estimate the nodal configurational forces.

3 Homogenization of Piezoelectric Material

In this section we will briefly describe the homogenization technique of the mechanical and electrical quantities and the material parameters of piezoelectric materials. Among the homogenization techniques, the FE^2 based homogenization is computationally efficient. FE^2 based homogenization is a two-scale homogenization, in which two boundary value problems are solved: one on the macro level and the other on the micro level. On the macro level no constitutive law is prescribed, but a boundary value problem on the micro level is used to determine the homogenized material response. To have representative numerical results on the macro level or to capture the effect of micro inhomogeneities on the macro problem, it is necessary to attach a micro domain to each macro

Gauss point. This micro domain should contain enough microstructural features of the material; therefore, it is usually called representative volume element (RVE), see Figure 3. To prescribe the relevant admissible boundary conditions for the RVEs, one needs to pass at each Gauss point either the macro displacement gradient and the macro electric field, or the macro stress tensor and the macro electric displacement down to the micro level. With the help of these boundary conditions, one solves the micro boundary value problem and determines the remaining quantities such as average stress tensor and electric displacement, or average displacement gradient and electric field, respectively. These averaged quantities are passed back to the macro level as the material response.

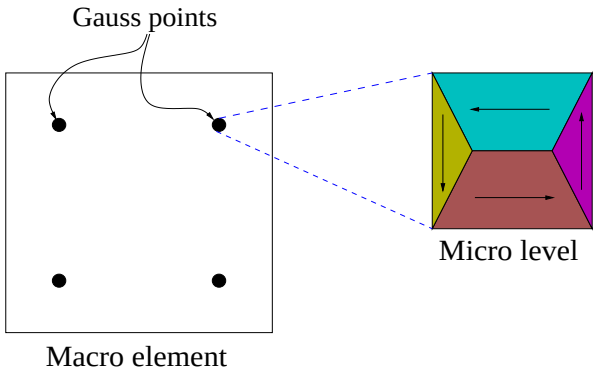

Figure 3: Macro-micro transition

In the present paper, the macro or averaged quantities are denoted by the symbols with over bar and the micro quantities by the non-marked symbols. In the absence of the body forces, volume charges and holes on the micro level, the transition between the macro and the micro quantities is given as

$$\overline{\boldsymbol{\varepsilon}} = \frac{1}{V}\int_{\partial\mathcal{B}_{\text{mic}}} \operatorname{sym}(\mathbf{u}\otimes\mathbf{n})\,\mathrm{d}\Gamma, \quad \overline{\boldsymbol{\sigma}} = \frac{1}{V}\int_{\partial\mathcal{B}_{\text{mic}}} \operatorname{sym}(\mathbf{t}\otimes\mathbf{x})\,\mathrm{d}\Gamma, \tag{15}$$

$$\overline{\mathbf{E}} = -\frac{1}{V}\int_{\partial\mathcal{B}_{\text{mic}}} \varphi\,\mathbf{n}\,\mathrm{d}\Gamma, \quad \text{and} \quad \overline{\mathbf{D}} = -\frac{1}{V}\int_{\partial\mathcal{B}_{\text{mic}}} Q\,\mathbf{x}\,\mathrm{d}\Gamma. \tag{16}$$

To have a comprehensive proof of the connection between the macro and the micro quantities, readers are referred to Schröder (2009).

3.1 Determination of the Admissible Boundary Conditions for Micro BVP Problem

To have a consistent transition between the macro and micro quantities, it is required to satisfy one kind of energy criterion which is so called the Hill-Mandel condition. As the piezoelectric material is an electro-mechanically coupled material, it has two parts in the Hill-Mandel condition. The mechanical and the electrical parts of Hill-Mandel condition are

$$\overline{\boldsymbol{\sigma}}:\dot{\overline{\boldsymbol{\varepsilon}}} = \frac{1}{V}\int_{\mathcal{B}_{\text{mic}}} \boldsymbol{\sigma}:\dot{\boldsymbol{\varepsilon}}\,\mathrm{d}\Omega \qquad \text{and} \qquad \overline{\mathbf{D}}\cdot\dot{\overline{\mathbf{E}}} = \frac{1}{V}\int_{\mathcal{B}_{\text{mic}}} \mathbf{D}\cdot\dot{\mathbf{E}}\,\mathrm{d}\Omega, \tag{17}$$

respectively. The Hill-Mandel condition for coupled problem assumes that the power of the mechanical and electrical contributions on macro level are equivalent to the volume average of the power of the mechanical and electrical contributions on micro level. By introducing $\mathcal{P}_1$ and $\mathcal{P}_2$, the Hill-Mandel conditions (17) can be reformulated

$$\mathcal{P}_1 = \frac{1}{V}\int_{\mathcal{B}_{\text{mic}}} \boldsymbol{\sigma}:\dot{\boldsymbol{\varepsilon}}\,\mathrm{d}\Omega - \overline{\boldsymbol{\sigma}}:\dot{\overline{\boldsymbol{\varepsilon}}} = 0 \qquad \text{and} \qquad \mathcal{P}_2 = \frac{1}{V}\int_{\mathcal{B}_{\text{mic}}} \mathbf{D}\cdot\dot{\mathbf{E}}\,\mathrm{d}\Omega - \overline{\mathbf{D}}\cdot\dot{\overline{\mathbf{E}}} = 0. \tag{18}$$

By the Gauss formula, the volume integrals in (18) can be transformed to the surface or boundary integrals. Taking the mechanical part as an example,

$$\overline{\boldsymbol{\sigma}}:\dot{\overline{\boldsymbol{\varepsilon}}} = \frac{1}{V}\int_{\mathcal{B}_{\text{mic}}} \boldsymbol{\sigma}:\dot{\boldsymbol{\varepsilon}}\,\mathrm{d}\Omega = \frac{1}{V}\int_{\partial\mathcal{B}_{\text{mic}}} \mathbf{t}\cdot\dot{\mathbf{u}}\,\mathrm{d}\Gamma. \tag{19}$$

Adding and subtracting the term $\overline{\boldsymbol{\sigma}}:\dot{\overline{\boldsymbol{\varepsilon}}}$ to the right hand side (RHS) of the first equation in (18) and using (19), $\mathcal{P}_1$ can be rewritten as

$$\mathcal{P}_1 = \frac{1}{V}\int_{\partial\mathcal{B}_{\text{mic}}} \mathbf{t}\cdot\dot{\mathbf{u}}\,\mathrm{d}\Gamma - \overline{\boldsymbol{\sigma}}:\dot{\overline{\boldsymbol{\varepsilon}}} - \overline{\boldsymbol{\sigma}}:\dot{\overline{\boldsymbol{\varepsilon}}} + \overline{\boldsymbol{\sigma}}:\dot{\overline{\boldsymbol{\varepsilon}}}. \tag{20}$$

Using the definitions of the average quantities or the boundary integral on the micro level, the mechanical power on macro level $\overline{\boldsymbol{\sigma}}:\dot{\overline{\boldsymbol{\varepsilon}}}$ can be expressed in three different ways as

$$\left.\begin{aligned}
\overline{\boldsymbol{\sigma}}:\dot{\overline{\boldsymbol{\varepsilon}}} &= \overline{\boldsymbol{\sigma}}:\frac{1}{V}\int_{\partial\mathcal{B}_{\text{mic}}} \operatorname{sym}[\dot{\mathbf{u}}\otimes\mathbf{n}]\mathrm{d}\Gamma = \frac{1}{V}\int_{\partial\mathcal{B}_{\text{mic}}} (\overline{\boldsymbol{\sigma}}\mathbf{n})\cdot\dot{\mathbf{u}}\mathrm{d}\Gamma,\\
\overline{\boldsymbol{\sigma}}:\dot{\overline{\boldsymbol{\varepsilon}}} &= \overline{\boldsymbol{\sigma}}:\dot{\overline{\operatorname{grad}\,\mathbf{u}}}\\
&= \frac{1}{V}\int_{\partial\mathcal{B}_{\text{mic}}} \operatorname{sym}[\mathbf{t}\otimes\mathbf{x}]\,\mathrm{d}\Gamma:\dot{\overline{\operatorname{grad}\,\mathbf{u}}} = \frac{1}{V}\int_{\partial\mathcal{B}_{\text{mic}}} \mathbf{t}\cdot(\dot{\overline{\operatorname{grad}\,\mathbf{u}}}\,\mathbf{x})\,\mathrm{d}\Gamma,\\
\overline{\boldsymbol{\sigma}}:\dot{\overline{\boldsymbol{\varepsilon}}} &= \overline{\boldsymbol{\sigma}}:\dot{\overline{\operatorname{grad}\,\mathbf{u}}}\\
&= (\overline{\boldsymbol{\sigma}}\frac{1}{V}\int_{\partial\mathcal{B}_{\text{mic}}} \mathbf{n}\otimes\mathbf{x}\,\mathrm{d}\Gamma):\dot{\overline{\operatorname{grad}\,\mathbf{u}}} = \frac{1}{V}\int_{\partial\mathcal{B}_{\text{mic}}} (\overline{\boldsymbol{\sigma}}\mathbf{n})\cdot(\dot{\overline{\operatorname{grad}\,\mathbf{u}}}\,\mathbf{x})\,\mathrm{d}\Gamma
\end{aligned}\right\}. \tag{21}$$

Inserting the different expressions of $\overline{\boldsymbol{\sigma}}:\dot{\overline{\boldsymbol{\varepsilon}}}$ into the right hand side of (20) and doing some mathematical manipulations, we get

$$\mathcal{P}_1 = \frac{1}{V}\int_{\partial\mathcal{B}_{\text{mic}}} \Big[\mathbf{t}\cdot\dot{\mathbf{u}} - (\overline{\boldsymbol{\sigma}}\mathbf{n})\cdot\dot{\mathbf{u}} - \mathbf{t}\cdot(\dot{\overline{\operatorname{grad}\,\mathbf{u}}}\,\mathbf{x}) + (\overline{\boldsymbol{\sigma}}\mathbf{n})\cdot(\dot{\overline{\operatorname{grad}\,\mathbf{u}}}\,\mathbf{x})\Big]\mathrm{d}\Gamma \tag{22}$$

$$= \frac{1}{V}\int_{\partial\mathcal{B}_{\text{mic}}} ((\mathbf{t}-\overline{\boldsymbol{\sigma}}\mathbf{n})\cdot(\dot{\mathbf{u}} - \dot{\overline{\operatorname{grad}\,\mathbf{u}}}\,\mathbf{x}))\,\mathrm{d}\Gamma. \tag{23}$$

As $\mathcal{P}_1 = 0$, one of the two terms of the multiplication under the boundary integral in (23) must be zero. Thus from equation (23) two types of mechanical boundary conditions for the micro boundary value problem (BVP) are deduced

$$\mathbf{t} = \overline{\boldsymbol{\sigma}}\mathbf{n} \qquad \text{or} \qquad \dot{\mathbf{u}} = \dot{\overline{\operatorname{grad}\,\mathbf{u}}}\,\mathbf{x} \quad \text{on} \quad \partial\mathcal{B}_{\text{mic}}. \tag{24}$$

Another possible mechanical boundary condition for the micro scale problem is called periodic boundary condition. This boundary condition allows a fluctuation of $\mathbf{u}$, i.e.

$$\dot{\mathbf{u}} = \dot{\overline{\operatorname{grad}\,\mathbf{u}}}\,\mathbf{x} + \dot{\widetilde{\mathbf{w}}} \qquad \Rightarrow \qquad \operatorname{grad}\dot{\mathbf{u}} = \dot{\overline{\operatorname{grad}\,\mathbf{u}}} + \operatorname{grad}\dot{\widetilde{\mathbf{w}}}, \tag{25}$$

where $\widetilde{\mathbf{w}}$ denotes the fluctuation of displacement field at micro scale away from homogeneous term $\overline{\operatorname{grad}\,\mathbf{u}}\,\mathbf{x}$. Suppose that the boundary of the representative volume element $\partial\mathcal{B}_{\text{mic}}$ can be divided into two parts: one positive boundary $\partial\mathcal{B}^+_{\text{mic}}$ and one negative boundary $\partial\mathcal{B}^-_{\text{mic}}$, whose normal vectors are related in $\mathbf{n}^+ = -\mathbf{n}^-$. With the assumption in (25), the equation (23) can be transformed to

$$\mathcal{P}_1 = \frac{1}{V}\int_{\partial\mathcal{B}_{\text{mic}}} (\mathbf{t}-\overline{\boldsymbol{\sigma}}\mathbf{n})\cdot(\dot{\widetilde{\mathbf{w}}})\,\mathrm{d}\Gamma \tag{26}$$

$$= \frac{1}{V}\left[\int_{\partial\mathcal{B}^+_{\text{mic}}} (\mathbf{t}^+ - \overline{\boldsymbol{\sigma}}\mathbf{n}^+)\cdot\dot{\widetilde{\mathbf{w}}}^+\,\mathrm{d}\Gamma + \int_{\partial\mathcal{B}^-_{\text{mic}}} (\mathbf{t}^- - \overline{\boldsymbol{\sigma}}\mathbf{n}^-)\cdot\dot{\widetilde{\mathbf{w}}}^-\,\mathrm{d}\Gamma\right]. \tag{27}$$

By further assuming equal fluctuation of the displacement field on the opposite boundaries of the $\mathcal{B}_{\text{mic}}$, i.e., $\widetilde{\mathbf{w}}^+ = \widetilde{\mathbf{w}}^-$, the equation (27) can be simplified to

$$\mathcal{P}_1 = \frac{1}{V}\left[\int_{\partial\mathcal{B}^+_{\text{mic}}} \mathbf{t}^+\cdot\dot{\widetilde{\mathbf{w}}}^+\,\mathrm{d}\Gamma + \int_{\partial\mathcal{B}^-_{\text{mic}}} \mathbf{t}^-\cdot\dot{\widetilde{\mathbf{w}}}^-\,\mathrm{d}\Gamma\right]. \tag{28}$$

To fulfill the Hill-Mandel condition $\mathcal{P}_1 = 0$ in equation (28), it follows that $\mathbf{t}^+ = -\mathbf{t}^-$. So we can write the mechanical periodic boundary condition for the $\mathcal{B}_{\text{mic}}$ as

$$\dot{\tilde{\mathbf{w}}}^+ = \dot{\tilde{\mathbf{w}}}^- \qquad \text{and} \qquad \mathbf{t}^+ = -\mathbf{t}^- \qquad \text{on the oposite faces of } \partial\mathcal{B}_{\text{mic}}. \tag{29}$$

Similarly, by using the electrical part of the Hill-Mandel condition, three boundary conditions for electrical balance equation can be determined, i.e. the Dirichlet b.c.

$$\dot{\varphi} = -\dot{\overline{\mathbf{E}}}\cdot\mathbf{x} \tag{30}$$

or the periodic b.c.

$$\begin{aligned} \dot{\varphi} &= -\dot{\overline{\mathbf{E}}}\cdot\mathbf{x} + \dot{\tilde{\omega}} \\ \dot{\tilde{\omega}}^+ &= \dot{\tilde{\omega}}^- \\ Q^+ &= -Q^- \end{aligned} \tag{31}$$

or Neumann b.c.

$$Q = -\overline{\mathbf{D}}\cdot\mathbf{n}. \tag{32}$$

For explicit derivation of the boundary conditions of the electrical part, see Schröder (2009).

3.2 Homogenized Material Moduli

For simplicity the formulation of the homogenized material parameters are described in detail only for the displacement boundary condition or the Dirichlet b.c. to the micro domain. In this section underlined symbols are used for the matrix notation with Voigt style. The constitutive relations of piezoelectric material in (8) and (9) can be expressed in a combined Voigt notation as

$$\begin{bmatrix} \underline{\boldsymbol{\sigma}} \\ \underline{\mathbf{D}} \end{bmatrix} = \begin{bmatrix} \underline{\mathbb{C}} & \underline{\mathbb{b}}^T \\ \underline{\mathbb{b}} & -\underline{\mathbf{A}} \end{bmatrix} \begin{bmatrix} \underline{\boldsymbol{\varepsilon}} \\ -\underline{\mathbf{E}} \end{bmatrix} + \begin{bmatrix} -\underline{\mathbb{C}}\,\underline{\boldsymbol{\varepsilon}}^0 \\ \underline{\mathbf{P}}^0 - \underline{\mathbb{b}}\,\underline{\boldsymbol{\varepsilon}}^0 \end{bmatrix}, \tag{33}$$

alternatively,

$$\underline{\mathbf{S}} = \underline{\mathbb{L}}\,\underline{\mathbf{e}} + \underline{\mathbf{e}}^0, \tag{34}$$

where

$$\underline{\mathbf{S}} = \begin{bmatrix} \underline{\boldsymbol{\sigma}} \\ \underline{\mathbf{D}} \end{bmatrix}, \quad \underline{\mathbb{L}} = \begin{bmatrix} \underline{\mathbb{C}} & \underline{\mathbb{b}}^T \\ \underline{\mathbb{b}} & -\underline{\mathbf{A}} \end{bmatrix}, \quad \underline{\mathbf{e}} = \begin{bmatrix} \underline{\boldsymbol{\varepsilon}} \\ -\underline{\mathbf{E}} \end{bmatrix} \quad \text{and} \quad \underline{\mathbf{e}}^0 = \begin{bmatrix} -\underline{\mathbb{C}}\,\underline{\boldsymbol{\varepsilon}}^0 \\ \underline{\mathbf{P}}^0 - \underline{\mathbb{b}}\,\underline{\boldsymbol{\varepsilon}}^0 \end{bmatrix}.$$

The prescribed boundary displacements and potentials on the micro domains are

$$\mathbf{u}_q = \overline{\text{grad}\,\mathbf{u}}\,\mathbf{x}_q = \overline{\boldsymbol{\varepsilon}}\,\mathbf{x}_q + \overline{\boldsymbol{\omega}}\,\mathbf{x}_q \tag{35}$$

$$\text{and} \quad \varphi_q = -\overline{\mathbf{E}}\cdot\mathbf{x}_q, \tag{36}$$

respectively, where $q = 1, \ldots, M$ (M is the total number of boundary nodes). In equation (35), $\overline{\boldsymbol{\varepsilon}}$ and $\overline{\boldsymbol{\omega}}$ are the symmetric and the anti-symmetric part of the displacement gradient tensor $\overline{\text{grad}\,\mathbf{u}}$, respectively. Introducing Voigt notation for the macro strain tensor in 2D problems $\underline{\overline{\boldsymbol{\varepsilon}}} = [\overline{\varepsilon}_{11},\ \overline{\varepsilon}_{22},\ 2\overline{\varepsilon}_{12}]^T$, the alternative representation of $\underline{\mathbf{u}}_q$ and φ_q are

$$\underline{\mathbf{u}}_q = \underline{\mathbb{Q}}_{qm}^T\,\underline{\overline{\boldsymbol{\varepsilon}}} + \underline{\mathbb{P}}_{qm}^T\,\overline{\boldsymbol{\omega}} \tag{37}$$

$$\varphi_q = -\underline{\mathbb{Q}}_{qe}^T(\underline{\overline{\mathbf{E}}}), \tag{38}$$

where $\underline{\mathbb{Q}}_{qm}$, $\underline{\mathbb{P}}_{qm}$ and $\underline{\mathbb{Q}}_{qe}$ are defined in the following way,

$$\underline{\mathbb{Q}}_{qm} = \frac{1}{2}\begin{bmatrix} 2x_1 & 0 \\ 0 & 2x_2 \\ x_2 & x_1 \end{bmatrix}_q, \quad \underline{\mathbb{Q}}_{qe} = \begin{bmatrix} x_1 \\ x_2 \end{bmatrix}_q, \quad \underline{\mathbb{P}}_{qm} = \begin{bmatrix} -x_2 & x_1 \end{bmatrix}_q. \tag{39}$$

As there is no contribution from the rotational part of the displacement gradient (the second term in (35)) to the stress field, we omit this term in the following formulations. In a combined way the generalized displacement vector is

$$\underline{\mathbf{u}}_{qc} = \underline{\mathbb{Q}}_{qc}^T \overline{\underline{\mathbf{e}}}, \tag{40}$$

where

$$\begin{aligned}
\underline{\mathbf{u}}_{qc} &= \left[u_{1q}, u_{2q}, \varphi_q\right]^T, && (41)\\
\overline{\underline{\mathbf{e}}} &= \left[\overline{\varepsilon}_{11}, \overline{\varepsilon}_{22}, 2\overline{\varepsilon}_{12}, -\overline{E}_1, -\overline{E}_2\right]^T, && (42)\\
\underline{\mathbb{Q}}_{qc} &= \begin{bmatrix} \underline{\mathbb{Q}}_{qm} & \mathbf{0} \\ \mathbf{0} & -\underline{\mathbb{Q}}_{qe} \end{bmatrix}. && (43)
\end{aligned}$$

The boundary displacements and the electric potentials in global form $\underline{\mathbf{u}}_b = \underline{\mathbb{Q}}_c^T \overline{\underline{\mathbf{e}}}$, where $\underline{\mathbf{u}}_b$ contains all boundary degrees of freedom (the boundary mechanical displacements and electrical potentials) and

$$\underline{\mathbb{Q}}_c = \left[\underline{\mathbb{Q}}_{1c}, \underline{\mathbb{Q}}_{2c}, \cdots, \underline{\mathbb{Q}}_{Mc}\right]. \tag{44}$$

Assume $\underline{\mathbf{K}}\ \underline{\mathbf{u}} = \underline{\mathbf{F}}$ is the linear system of equations on the micro level after performing the assembling in the Finite Element Analysis (FEA). The stiffness matrix $\underline{\mathbf{K}}$, the displacement vector $\underline{\mathbf{u}}$ and the right hand side $\underline{\mathbf{F}}$ are partitioned as

$$\begin{bmatrix} \underline{\mathbf{K}}_{ii} & \underline{\mathbf{K}}_{ib} \\ \underline{\mathbf{K}}_{bi} & \underline{\mathbf{K}}_{bb} \end{bmatrix} \begin{bmatrix} \underline{\mathbf{u}}_i \\ \underline{\mathbf{u}}_b \end{bmatrix} = \begin{bmatrix} \underline{\mathbf{F}}_i \\ \underline{\mathbf{F}}_b \end{bmatrix}, \tag{45}$$

where the indices i and b denote the internal and the boundary degrees of freedom, respectively.

And the linear displacements and potentials on the boundary can be represented in the compact global combined form

$$\mathbf{d}(\underline{\mathbf{u}}_b; \overline{\underline{\mathbf{e}}}) = \underline{\mathbf{u}}_b - \underline{\mathbb{Q}}_c^T \overline{\underline{\mathbf{e}}} = \mathbf{0}. \tag{46}$$

Using the Lagrange multiplier method to incorporate the boundary constraints in the total energy of the discrete system, one has

$$\pi = \frac{1}{2}\underline{\mathbf{u}}^T \underline{\mathbf{K}}\underline{\mathbf{u}} - \underline{\mathbf{u}}^T \underline{\mathbf{F}} - \underline{\boldsymbol{\delta}}^T (\underline{\mathbf{u}}_b - \underline{\mathbb{Q}}_c^T \overline{\underline{\mathbf{e}}}), \tag{47}$$

where $\underline{\boldsymbol{\delta}}$ is the Lagrange multiplier. To have the equilibrium solution of the system, the following conditions must be satisfied

$$\frac{\partial \pi}{\partial \underline{\mathbf{u}}} := \mathbf{0} \quad \text{and} \quad \frac{\partial \pi}{\partial \underline{\boldsymbol{\delta}}} := \mathbf{0}. \tag{48}$$

Determining the partial derivatives in (48), it is possible to deduce the following equations,

$$\begin{aligned}
&\underline{\mathbf{K}}_{ii}\underline{\mathbf{u}}_i + \underline{\mathbf{K}}_{ib}\underline{\mathbf{u}}_b - \underline{\mathbf{F}}_i = \mathbf{0} \\
&\underline{\mathbf{K}}_{bi}\underline{\mathbf{u}}_i + \underline{\mathbf{K}}_{bb}\underline{\mathbf{u}}_b - \underline{\mathbf{F}}_b - \underline{\boldsymbol{\delta}} = \mathbf{0} \\
&\underline{\mathbf{u}}_b - \underline{\mathbb{Q}}_c^T \overline{\underline{\mathbf{e}}} = \mathbf{0}.
\end{aligned} \tag{49}$$

The average or homogenized stress tensor and electric displacement in a combined way with the help of Voigt notation is expressed in the following way,

$$\overline{\underline{\mathbf{S}}} = \frac{1}{V}\underline{\mathbb{Q}}_c \underline{\boldsymbol{\delta}}, \tag{50}$$

where $\overline{\underline{\mathbf{S}}} = \left[\overline{\sigma}_{11}, \overline{\sigma}_{22}, \overline{\sigma}_{12}, \overline{D}_1, \overline{D}_2\right]^T$. Eliminating $\underline{\boldsymbol{\delta}}$ from the second equation in (49) and (50) and using the first equation in (49), one has

$$\begin{aligned}
\overline{\underline{\mathbf{S}}} &= \frac{1}{V}\underline{\mathbb{Q}}_c \left(\underline{\mathbf{K}}_{bi}\underline{\mathbf{u}}_i + \underline{\mathbf{K}}_{bb}\underline{\mathbf{u}}_b - \underline{\mathbf{F}}_b\right) && (51)\\
&= \frac{1}{V}\underline{\mathbb{Q}}_c \left(\underline{\mathbf{K}}_{bi}\underline{\mathbf{K}}_{ii}^{-1}(\underline{\mathbf{F}}_i - \underline{\mathbf{K}}_{ib}\underline{\mathbf{u}}_b) + \underline{\mathbf{K}}_{bb}\underline{\mathbf{u}}_b - \underline{\mathbf{F}}_b\right) && (52)\\
&= \frac{1}{V}\underline{\mathbb{Q}}_c \left((\underline{\mathbf{K}}_{bb} - \underline{\mathbf{K}}_{bi}\underline{\mathbf{K}}_{ii}^{-1}\underline{\mathbf{K}}_{ib})\underline{\mathbf{u}}_b + \underline{\mathbf{K}}_{bi}\underline{\mathbf{K}}_{ii}^{-1}\underline{\mathbf{F}}_i - \underline{\mathbf{F}}_b\right) && (53)\\
&= \frac{1}{V}\underline{\mathbb{Q}}_c \left((\underline{\mathbf{K}}_{bb} - \underline{\mathbf{K}}_{bi}\underline{\mathbf{K}}_{ii}^{-1}\underline{\mathbf{K}}_{ib})\underline{\mathbb{Q}}_c^T \overline{\underline{\mathbf{e}}} + \underline{\mathbf{K}}_{bi}\underline{\mathbf{K}}_{ii}^{-1}\underline{\mathbf{F}}_i - \underline{\mathbf{F}}_b\right) && (54)\\
&= \frac{1}{V}\underline{\mathbb{Q}}_c \widetilde{\underline{\mathbf{K}}}_{bb}\underline{\mathbb{Q}}_c^T \overline{\underline{\mathbf{e}}} + \frac{1}{V}\underline{\mathbb{Q}}_c \widetilde{\underline{\mathbf{F}}}_b. && (55)
\end{aligned}$$

Comparison between the equations (34) and (55) leads to

$$\underline{\mathbb{L}} = \frac{1}{V}\underline{\mathbb{Q}}_c\underline{\widetilde{\mathbf{K}}}_{bb}\underline{\mathbb{Q}}_c^T \qquad \text{and} \qquad \underline{\mathbf{e}}^0 = \frac{1}{V}\underline{\mathbb{Q}}_c\underline{\widetilde{\mathbf{F}}}_b, \tag{56}$$

where

$$\underline{\widetilde{\mathbf{K}}}_{bb} = \underline{\mathbf{K}}_{bb} - \underline{\mathbf{K}}_{bi}\underline{\mathbf{K}}_{ii}^{-1}\underline{\mathbf{K}}_{ib} \quad \text{and} \quad \underline{\widetilde{\mathbf{F}}}_b = \underline{\mathbf{K}}_{bi}\underline{\mathbf{K}}_{ii}^{-1}\underline{\mathbf{F}}_i - \underline{\mathbf{F}}_b. \tag{57}$$

For the complete derivation of the homogenized material parameters (only mechanical part), readers are referred to Miehe and Koch (2002). From equation (56) the homogenized material parameters, elasticity modulus $\underline{\mathbb{C}}$, dielectric modulus $\underline{\mathbf{A}}$, piezoelectric modulus $\underline{\mathbb{b}}$, remanent strain $\underline{\boldsymbol{\varepsilon}}^0$ and remanent polarization $\underline{\mathbf{P}}^0$ can easily be determined.

3.3 Homogenization of Configurational Forces

Because of the inhomogeneities of the material, it is essential to homogenize the Eshelby stress tensor to capture the effects of the micro discontinuities to the configurational forces on the macro level. There are several approaches to determine the homogenized Eshelby stress tensor, see Ricker et al. (2010). In this work the direct approach is used to determine the homogenized Eshelby stress tensor which is volume average of the Eshelby stress tensor on micro level

$$\begin{aligned} \overline{\boldsymbol{\Sigma}} &= \frac{1}{V}\int_{\mathcal{B}_{\text{mic}}} \boldsymbol{\Sigma}\, \mathrm{d}\Omega \\ &= \frac{1}{V}\int_{\mathcal{B}_{\text{mic}}} \left[H\mathbf{1} - (\operatorname{grad}\mathbf{u})^T\boldsymbol{\sigma} - \operatorname{grad}\varphi \otimes \mathbf{D}\right] \mathrm{d}\Omega. \end{aligned} \tag{58}$$

The homogenized Eshelby stress tensor can also be computed using averaged mechanical and electrical quantities as

$$\overline{\boldsymbol{\Sigma}}^* = \overline{H}\,\mathbf{1} - (\overline{\operatorname{grad}\mathbf{u}})^T\overline{\boldsymbol{\sigma}} - \overline{\operatorname{grad}\varphi} \otimes \overline{\mathbf{D}}, \tag{59}$$

but this averaged Eshelby stress tensor $\overline{\boldsymbol{\Sigma}}^*$ does not satisfy the Hill-Mandel condition. Ricker et al. (2010) showed for large strain problem that it does not satisfy the Hill-Mandel condition or it needs some extra terms to satisfy the Hill-Mandel condition.

Using the averaged Eshelby stress tensor $\overline{\boldsymbol{\Sigma}}$, the nodal configurational forces on macro level can be determined. The configurational force at node J on macro level is

$$\mathbf{G}^J = \bigcup_{e\,=\,1}^{n_{\text{el}}^*} \int_{\Omega_e} \overline{\boldsymbol{\Sigma}}\, \operatorname{grad} N^J\, \mathrm{d}\Omega, \tag{60}$$

where n_{el}^* is the total number of adjacent elements to node J.

4 Numerical Results and Analysis

In this work the main focus is to establish a numerical technique which is capable of capturing the effect of micro inhomogeneities of the piezoelectric materials on the macro responses. Here the configurational forces at the crack tip of the macro domain are used as the macro response. We attempted to figure out the influence of the underlying microstructure on the configurational force at the crack tip of a macro specimen. An extensive investigation is done to understand the influence of the external electric field on the configurational forces at the crack tip. In a real life problem the underlying microstructures containing domains, domain walls, grains, grain boundaries, micro defects, etc. are very complex in nature. If we want to capture the influences of the whole scenario of the underlying microstructures, it is computationally very expensive or in some cases it is impossible. But to understand the characteristic behaviour of the microstructures, it is sufficient to restrict attention to simplified micro domains with different orientations of the domains, domain walls, micro cracks, grains, etc.

4.1 Macro Geometry and Microstructure

A 4 mm×4 mm macro specimen with a sharp crack (see in Figure 4) is simulated to determine the configurational forces at the crack tip with different micro domains at every Gauss point of the macro domain. The length of the crack is 2 mm and the width of the crack at the opening is 0.1 mm. In all simulations the bottom boundary of the macro domain remains fixed and the top boundary is displaced by 0.2 mm. Three different electric field situations are taken into account to simulate the problem: no external electric field, external upward electric field and external downward electric field. These electric field situations are realized by applying the electric potentials on the top and the bottom boundaries (see in Figure 4) of the macroscopic specimen. Here, the crack in the macro specimen is modelled as electrically impermeable crack.

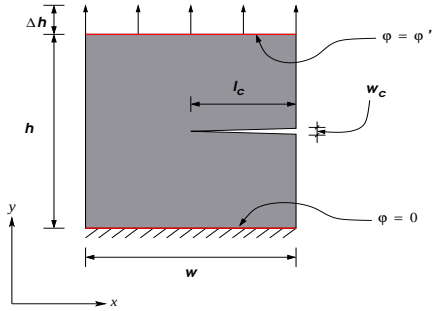

Figure 4: *A macro fractured specimen with dimension $h \times w$ containing a sharp crack (with crack length l_c and width at the opening w_c). The top of the structure is displaced with Δh and the applied potentials on the top and the bottom are φ' and 0, respectively.*

4.2 Material Parameters

In the following all the simulations are done for poled soft lead zirconate titanate ceramics. The material parameters in Voigt notation are given in the following:

$$\begin{aligned} \underline{\mathbb{C}} &= \begin{bmatrix} 12.6 & 5.3 & 0.0 \\ 5.3 & 11.7 & 0.0 \\ 0.0 & 0.0 & 3.53 \end{bmatrix} \cdot 10^4 \frac{\mathrm{N}}{\mathrm{mm}^2} \\ \underline{\mathbb{b}} &= \begin{bmatrix} 0.0 & 0.0 & 17.0 \\ -6.5 & 23.3 & 0.0 \end{bmatrix} \cdot 10^{-6} \frac{\mathrm{C}}{\mathrm{mm}^2} \\ \underline{\mathbf{A}} &= \begin{bmatrix} 1.51 & 0.0 \\ 0.0 & 1.3 \end{bmatrix} \cdot 10^{-11} \frac{\mathrm{C}}{\mathrm{Vmm}}. \end{aligned} \tag{61}$$

These material data are acquired from McMeeking and Ricoeur (2003). This data set prescribes a material which is poled in the direction of positive y-axis. The polarization in positive y-direction is also considered by assigning

$$\underline{\boldsymbol{\varepsilon}}^0 = [-0.0039 \quad 0.0076 \quad 0.0]^T \quad \text{and} \quad \underline{\mathbf{P}}^0 = [0.0 \quad 0.2]^T \cdot 10^{-6} \frac{\mathrm{C}}{\mathrm{mm}^2}. \tag{62}$$

For the material poled with other orientations, the material parameters are transformed with the multiplication of the corresponding rotation matrices.

4.3 Configurational Force on the Micro Domain

To determine the boundary conditions of the micro domain, the displacement gradient and the electric field from the macro problem are provided to the micro BVP. Using equations (24) and (30) the displacements and the potentials on the boundary of the micro domain are determined. Equations (24) and (30) give the displacement type b.c. or the Dirichlet b.c for the micro domain. To simulate this micro problem, the following displacement gradient and electric field are used,

$$\overline{\text{grad}\,\mathbf{u}} = \begin{bmatrix} 0.1 & 0.05 \\ 0.07 & 0.15 \end{bmatrix} \quad \text{and} \quad \overline{\mathbf{E}} = \begin{bmatrix} 0 \\ 5 \end{bmatrix} \cdot 10^5 \frac{\mathrm{V}}{\mathrm{mm}}.$$

The micro domain (in Figure 5a)) with three domains and two vertical domain walls is simulated. The central domain is poled downward and other two domains are poled upward. Figure 5b) shows the nodal configurational forces (arrows) on the domain walls. Additionally, large configurational forces, which are not plotted in Figure 5b), appear on the boundary of the micro domain.

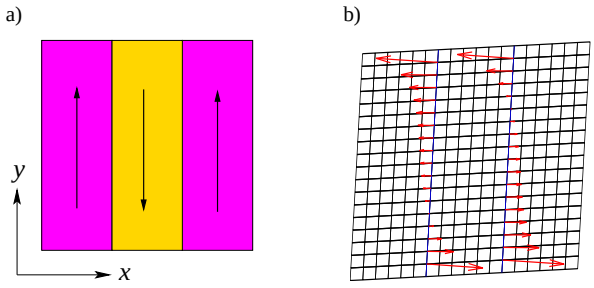

Figure 5: *Configurational forces on the domain walls of the microstructure: a) domain structure, b) configurational forces*

4.4 Influence of Different Microstructures without External Electric Field

Figure 6a) - 6d) show the stress and the electric field distributions in the macro specimen which is simulated with the homogenized material parameters. At the crack tip of this macro specimen, one can see the stress or the electric field singularities. These are the reason for the appearance of a large configurational force at the crack tip. And it may lead to crack propagation in the opposite direction of the configuration force (energy release).

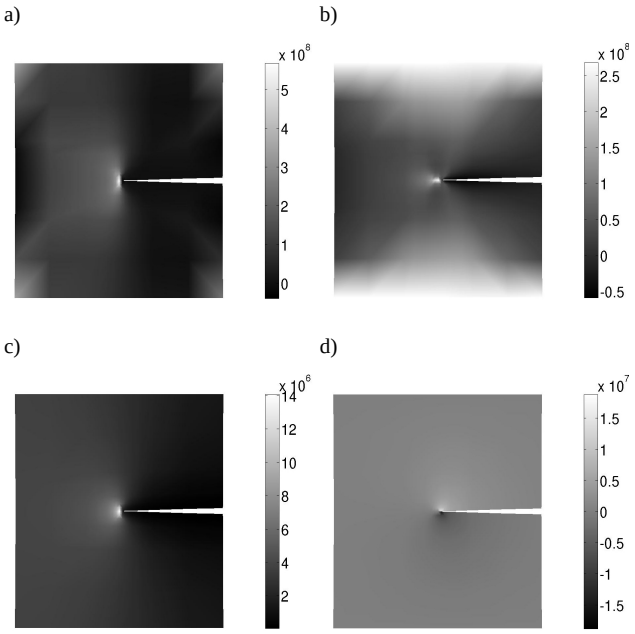

Figure 6: *Stress and electric field distributions on macroscopic specimen:* a) σ_{yy} *component of the stress tensor in* $\left(\frac{\mathrm{N}}{\mathrm{m}^2}\right)$, b) σ_{xx} *component of the stress tensor in* $\left(\frac{\mathrm{N}}{\mathrm{m}^2}\right)$, c) $\mathbf{E}_y$ *component of the electric field in* $\left(\frac{\mathrm{V}}{\mathrm{m}}\right)$, d) $\mathbf{E}_x$ *component of the electric field in* $\left(\frac{\mathrm{V}}{\mathrm{m}}\right)$

In Figure 7 and 8, the pictures on the top are the corresponding micro domains which are assigned to each Gauss point of the macro domain, and in the second row the deformed macro domains with configurational forces at the crack tip are displayed. At the bottom the numerical values of the configuration forces at the crack tip are reported. The arrows at the crack tips of the macro domains indicate the direction and the value of the configurational forces at the crack tip. The significance of the configurational forces is that the crack propagates in the opposite direction of the configurational force.

Figure 7a) shows that when the assigned micro domain is homogeneous and poled upward, there is a horizontal configurational force of 608.48 N. In Figure 7b) the assigned micro domain has three domains with two vertical 180° domain walls. The two outer domains are poled upward and the middle domain is poled downward. In this case the configurational force is approximately the same as in the previous case. The reason for this is that the elasticity tensor does not change, when the remanent polarization switches to the opposite direction. Thus the material response remains unchanged, when no external electric field is applied. In Figure 7c) the corresponding micro domain has three domains and two horizontal 90° domain walls, here the polarizations are inclined by 45°. In this case we get a upward inclined configurational force with a y-component of 34.894 N and x-component of 745.30 N. It means that the crack may move in an inclined direction with respect to the x-axis.

In Figure 8a), the assigned micro domain is homogeneous and horizontally poled in the positive x-axis. In this case, a horizontal configurational force of 879.19 N, which is larger than the configurational force in Figure 7a), is produced at the crack tip. Similar to Figure 7a) or 7b), Figure 8b) gives an almost identical configurational force as in Figure 8a). In Figure 8c) the assigned micro domain comprises three domains of inclined polarity and two vertical 90° domain walls. In this case one gets a similar configurational force as in Figure 7c). In Figure 8d) the microstructure has four domains: two are horizontally poled and the other two are vertically poled. It results in four 90° domain walls. In this case, the configurational force has an x-component of 793.62 N and no y-component.

It is worthwhile pointing out the two extreme cases of configurational forces: when the polarization is horizontally poled, it gives the maximum value of the configurational force and when it is vertically poled, it gives the minimum value of the configurational force. The other cases report an intermediate value of the configurational forces between the two extreme values. The coefficients of the elasticity tensor in the poling direction are with lower values, it means that the material is more rigid in the transverse direction to the polarization than in the poling direction. For that reason, the minimum configurational force is obtained, when the mechanical displacement is applied along the poling direction.

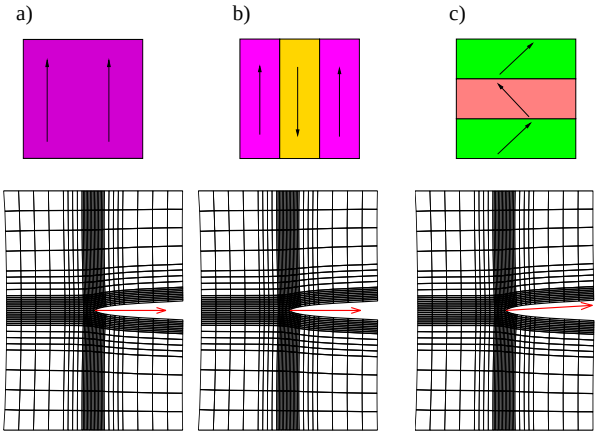

$$\mathbf{G} = \begin{bmatrix} 608.48 \\ 0.000 \end{bmatrix} \text{N}, \quad \mathbf{G} = \begin{bmatrix} 608.53 \\ 0.000 \end{bmatrix} \text{N}, \quad \mathbf{G} = \begin{bmatrix} 745.30 \\ 34.894 \end{bmatrix} \text{N}$$

Figure 7: *Configurational forces for different microstructures without external electric field*

4.5 Influence of External Electric Field

In this section the simulations are carried out for different external electric field conditions. In each example, results are compared for three cases: merely mechanical loading, mechanical along with upward external electric field, and mechanical along with downward external electric field. In Figure 9 the simulations are performed with a micro domain poled in the direction of the mechanical displacement. Simulations without an external electric field exhibit a horizontal configurational force of 608.16 N, while simulation with an upward external electric field results in a smaller horizontal configurational force of 278.66 N. Meanwhile the simulations with a downward electric field give also a smaller horizontal configurational force of 293.80 N. It is noticeable that for both upward and downward external electric fields the configurational forces are reduced by more than 50%.

In Figure 10 the simulations are done for a micro domain poled in the transverse direction to the mechanical

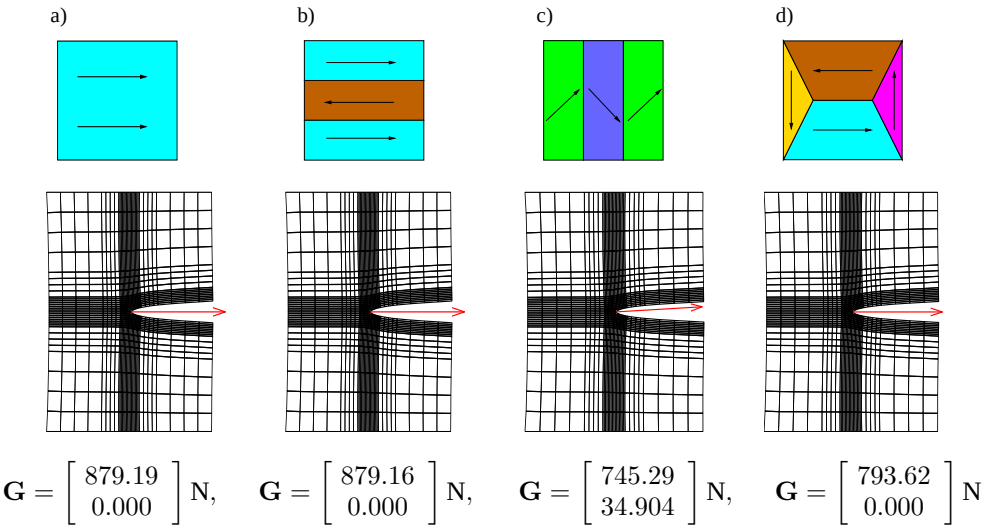

Figure 8: *Configurational forces for different microstructures without external electric field*

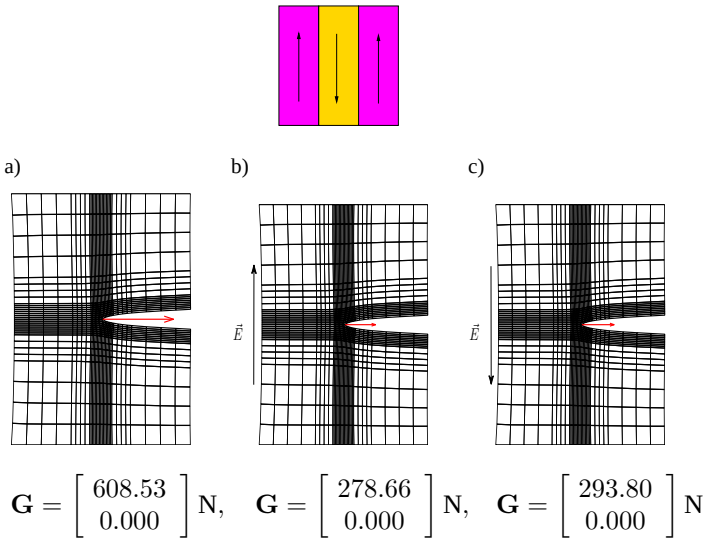

Figure 9: *Configurational forces for different electric loading conditions*

displacement. The simulation without an external electric field gives a horizontal configurational force of 879.16 N. The simulation with an upward external electric field reduces the configurational force by a significant amount and it produces a small positive y-component. Similarly, in the simulation with a downward external electric field the configurational force is reduced and a small negative y-component in the configurational force is obtained. It is also noted that there is a reduction of the configurational force in presence of either upward or downward electric field. The reduction is about 50%.

All previous simulations are done for the simple micro domains. These micro domains may not represent the real situations of the micro inhomogeneities of piezo-ceramics. However, the microstructures in real problems are featured with complex inhomogeneities, for example with domains, domain walls, micro cracks, grains, grain boundaries, etc. With an attempt to get closer to real situations of the micro inhomogeneities, the micro domain in Figure 11 is used to simulated the macro domain. In this micro domain we see five grains of piezoelectric materials enclosed by boundaries. In the grains we see domains and domain walls. When the simulation is done only for mechanical displacement, we get a configurational force with an x-component of 741.97 N and a y-component of -33.168 N. These values favor that the crack may propagate in an inclined direction to the x-axis. When it is simulated with an external electric field, both for the positive and the negative electric field in y-axis direction, the configurational forces are reduced to an x-component of 386 N and and a y-component of -26 N. The amounts

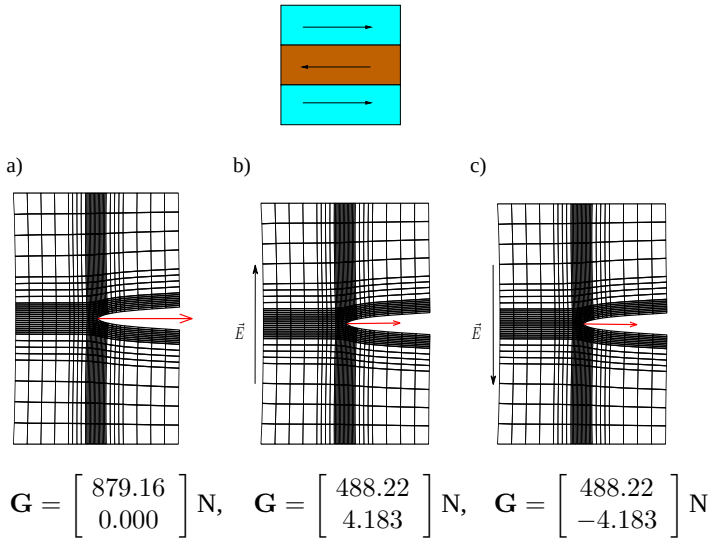

Figure 10: *Configurational forces for different electric loading conditions*

of reduction in the components of the configurational force are not exactly equal. For that reason the crack will propagate in a slightly different direction.

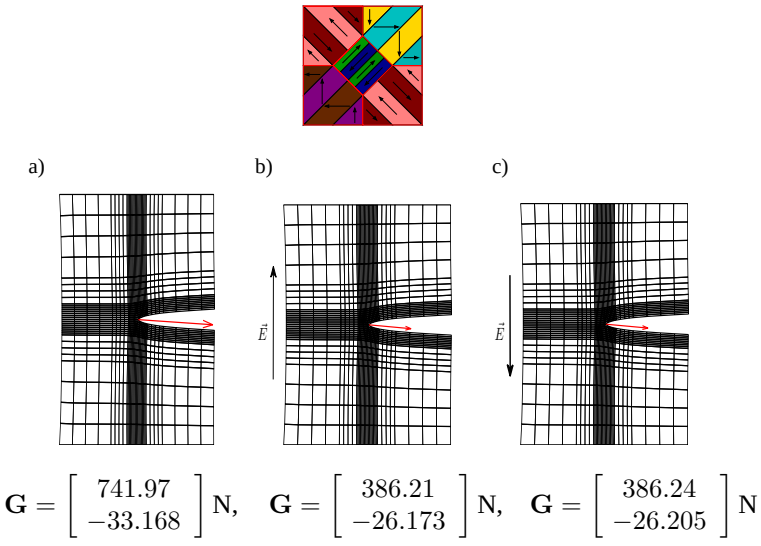

Figure 11: *Configurational forces for different electric loading conditions*

In Figure 12 the configurational forces for different micro domains and different external electric field conditions are summarized.

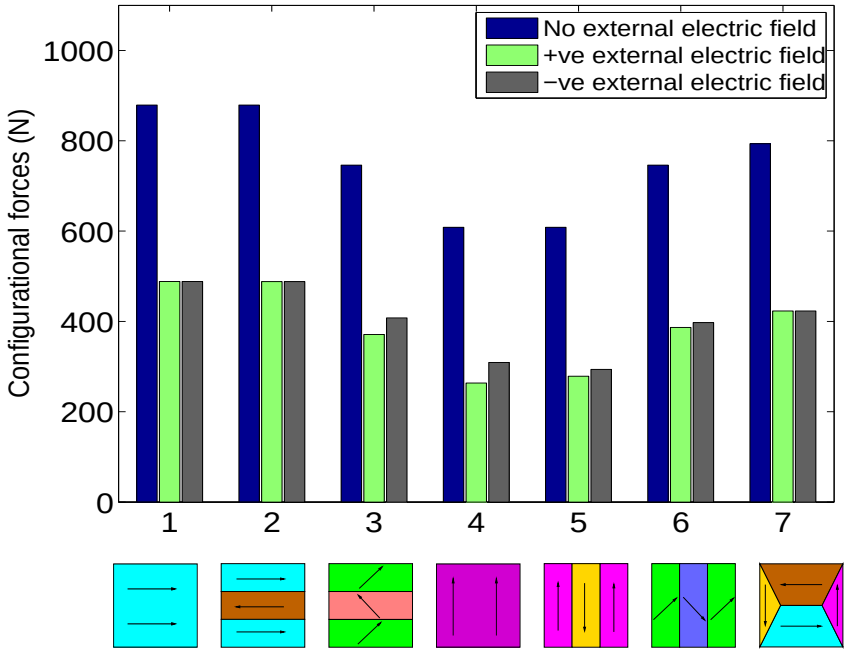

Figure 12: *Configurational forces for different microstructures with different electric loading conditions*

5 Conclusion

We have presented a homogenization technique for piezoelectric material, which is an electro-mechanically coupled material. Special emphasis has been given to the homogenization of the electromechanical Eshelby stress tensor for the determination of the configurational force at a crack tip on macro level. In case of FE^2 based computational homogenization, one can assign three different types of boundary conditions to solve micro BVP of piezoelectric material. For simplicity displacement types or Dirichlet boundary conditions for the homogenization were used. A macro specimen with a horizontal sharp crack has been simulated. To observe the effect of the micro inhomogeneities on the crack tip configurational force on macro level, simulations with several micro domains containing different inhomogeneities assigned to the Gauss points of macro domain were performed. In case of a horizontal or a vertical polarization in the micro domain, we got a configurational force parallel to the crack center line. Configurational forces slightly inclined to the crack center line were found in case of inclined polarization. An upper and a lower bound for the configurational force for purely mechanical loading on macro level were observed. When the mechanical displacement is along the polarization of the micro domain, the lower bound was obtained. And in case of the mechanical displacement transverse to the polarization, the upper bound is found, because piezoelectric material is stiffer in the transverse direction to the polarization. If an electric field is applied together with a mechanical displacement, the value of the configurational force reduces significantly for both positive and negative electric fields. The amount of the reduction is different for different micro domains.

In all cases we neglected possible movement of the domain walls, but in practical situation the domain wall moves in order to lower the total energy of the system. Meanwhile, rather simplified microstructures are used, which do not represent the real microstructures of the piezoelectric materials. When simulating the problem with a complex microstructure including grains, the grain boundary was modelled as a coherent and uncharged interface, as farther physical information on the nature of grain boundaries in piezoelectric materials is not yet available to the authors. The configurational force at the crack tip was investigated only for mode-I type crack. In future we will focus attention to configurational force at the crack tip using evolving micro domains by movement of domain walls. The homogenization will be carried out for other types of boundary conditions assigned to the micro domains. Furthermore, we will try to model the grain boundary of the piezoelectric material and simulate the specimen for other types of crack situations, e.g., mode-II, mode-III cracks.

References

Braun, M.: *Configurational forces induced by finite-element discretization*. *Proc. Estonian Acad. Sci. Phys. Math.*, 46(1/2), (1997), 24–31.

Eshelby, J. D.: *The force on an elastic singularity*. *Phil. Trans. Roy. Soc. London A*, 244, (1951), 87–112.

Eshelby, J. D.: *Energy relations and the energy-momentum tensor in continuum mechanics*. In: *Inelastic Behavior of Solids (eds M. F. Kanninen, W. F. Adler, A. R. Rosenfield and R. I. Jaffee)*, pages 77–115 (1970).

Gurtin, M. E.: *The Nature of Configurational Forces*. *Arch. Rational Mech. Anal.*, 131, (1995), 67–100.

Gurtin, M. E.: *Configurational forces as basic concept of continuum physics*. Springer, New York, Berlin, Heidelberg (2000).

Hill, R.: *On constitutive macro-variables for heterogeneous solids at finite strain*. *Proc. Roy. Soc. Lond. A*, 326, (1972), 131–147.

Kanouté, P.; Boso, D. P.; Chaboche, J. L.; Schrefler, B. A.: *Multiscale Methods for Composites: A Review*. *Archive of Computer Methods in Engineering*, 16, (2009), 31–77.

Kienzler, R.; Herrmann, G.: *Mechanics in Material Space*. Springer, New York, Berlin, Heidelberg (2000).

Leo, P. H.; Sekerka, R. F.: *The effect of surface stress on crystal-melt and crystal-crystal equilibrium*. *Acta metallurgica*, 37(12), (1989), 3119–3138.

Maugin, G. A.: *Material Inhomogeneities in Elasticity*. Chapman & Hall, London, Glasgow, New York, Tokyo, Melbourne, Madras (1993).

Maugin, G. A.: *Configurational forces: thermomechanics, physics, mathematics, and numerics*. CRC series–modern mechanics and mathematics, Taylor and Francis (2010).

McMeeking, R.; Ricoeur, A.: *The weight function for cracks in piezoelectrics*. *International Journal of Solids and Structures*, 40, (2003), 6143–6162.

Miehe, C.; Koch, A.: *Computational micro-to-macro transitions of discretized microstructures undergoing small strains*. *Archive of Applied Mechanics*, 72, (2002), 300–317.

Müller, R.; Gross, D.; Lupascu, D. C.: *Driving forces on domain walls in ferroelectric materials and interaction with defects*. *Computational Materials Science*, 35, (2006), 42–52.

Müller, R.; Kolling, S.; Gross, D.: *On Configurational forces in the context of the finite element method*. *International Journal of Numerical Methods in Engineering*, 53, 7, (2002), 1557–1575.

Müller, R.; Maugin, G. A.: *On Material Forces and Finite Element Discretizations*. *Computational Mechanics*, 29, 1, (2002), 52–60.

Nemat-Nasser, S.; Hori, M.: *Micromechanics: Overall properties of heterogeneous materials*. North-Holland, Amsterdam, London, New York, Tokyo (1993).

Qin, Q.: *Fracture mechanics of piezoelectric materials*. WIT Press, Southamton (2001).

Rice, J. R.: *A path independent integral and the approximate analysis of strain concentrations by notches and cracks*. *Journal of Applied Mechanics*, 35, (1968), 379–386.

Ricker, S.; Mergheim, J.; Steinmann, P.; Müller, R.: *A Comparison of Different Approaches in the Multi-Scale Computation of Configurational Forces*. *International Journal of Fracture*, 166, 1–2, (2010), 203–214.

Schrade, D.; Müller, R.; Gross, D.; Utschig, T.; Shur, V. Y.; Lupascu, D. C.: *Interaction of domain walls with defects in ferroelectric materials*. *Mechanics of Materials*, 39, (2007), 161–174.

Schröder, J.: *Derivation of the localization and homogenization conditions for electro-mechanically coupled problems*. *Computational Materials Science*, 46, (2009), 595–599.

Schröder, J.; Keip, M.-A.: *A Framework for the Two-Scale Homogenization of Electro-Mechanically Coupled Boundary Value Problems, Advanced Structured Materials (1): Computer Methods in Mechanics*. Springer (2010).

Schröder, J.; Keip, M.-A.: *Multiscale Modeling of Electro-mechanically Coupled Materials: Homogenization Procedure and Computation of Overall Moduli*. *IUTAM Symposium on Multiscale Modelling of Fatigue, Damage and Fracture in Smart Materials*, 24 of IUTAM Bookseries, (2011), 265–276.

Xu, Y.: *Ferroelectric Materials and Their Applications*. Elsevier Science Publishers B.V., Holland (1991).

Addresses:
M.Sc. Md Khalaquzzaman, Prof. Dr.-Ing. Ralf Müller, Institute of Applied Mechanics, University of Kaiserslautern, P.O. Box 3049, 67653 Kaiserslautern, Germany
email: khalaquz@rhrk.uni-kl.de, ram@rhrk.uni-kl.de
J.Prof. Ph.D. Bai-Xiang Xu, Mechanics of Functional Materials, Institute of Materials Science, FB 11, TU Darmstadt, Germany
email: xu@mfm.tu-darmstadt.de
Dr.-Ing. Sarah Ricker, Department of Flow and Material Simulation, Fraunhofer Institute for Industrial Mathematics, Kaiserslautern, Germany
email: sarah.ricker@itwm.fraunhofer.de